Traffic flow: A statistical physics point of view

Andreas Schadschneider

Institut für Theoretische Physik, Universität zu Köln, D-50923 Köln, Germany

Abstract

The investigation of traffic flow problems has a long tradition and various methods and approaches have been applied. In this review we focus on statistical mechanics and nonequilibrium aspects. It is shown that many properties of traffic flow can be modelled successfully by using rather simple cellular automaton models. Analytical methods for the investigation of discrete models are presented in some detail. Apart from highway traffic, also the modelling of city traffic and pedestrian dynamics will be discussed.

Key words: Nonequilibrium physics, cellular automata, complex systems
PACS: 45.70.Vn, 02.50.Ey, 05.40.-a, 05.60.-k

1 Introduction

The investigation of traffic flow has attracted the interest of physicists already a long time ago. Two aspects have to be distinguished. First there are obvious practical applications. The problems caused by traffic affect our everyday life since mobility has become an important factor. The traffic load has increased steadily over the past decades and often it is no longer possible to deal with this by building more streets. The consequence are annoying traffic jams. An alternative is the optimization of the existing traffic network which requires a detailed understanding of the properties of traffic flow.

The other aspect concerns physics. Traffic usually has to be treated as a nonequilibrium system. Due to its complexity many interesting collective effects occur. In fact traffic flow can be seen as the prototype of so-called driven systems which are far from equilibrium.

[1] E-mail: as@thp.uni-koeln.de

In this review we focus on the physics aspects of traffic. Especially the relation with statistical physics will be emphasized by considering cellular automata models. It should be pointed out that many other methods from physics have been used successfully in that field. For a more complete overview we refer to two recent comprehensive reviews [1,2] which cover the topic and related areas rather extensively. In [3] empirical results are discussed. Those interested in details of applications to real world problems should consult [4]. The series [5–7] covers also related flow problems in other fields.

2 Empirical results

The situation concerning empirical data is rather different from traditional areas of physics since no controlled experiments can be performed on traffic systems. Like in quantum mechanics performing an experiment can be a serious invasion into the system. Also creating a traffic jam on a highway just for research purposes will certainly not be appreciated by most drivers! We therefore have to rely mostly on passively observing everyday traffic situations.

Most traffic data are collected by stationary induction loops. A detector consist of two loops in close distance. It can in principle only measure times or time differences from which the quantities of interest have to be derived, e.g. the flow or the velocity. The flow J is given by the number of cars $N(T)$ passing the detector per time interval T, i.e. $J = \frac{1}{T}N(T)$. The velocity can be derived from the time interval needed to cross the loops. Other quantities that can be obtained are the length of the vehicle or the temporal and spatial headways between cars, i.e. the time interval between the signals of consecutive cars and the spatial distance between them. A big problem, however, is the determination of the density. Most detectors are event-driven and therefore only moving cars can be detected. Often one uses the hydrodynamic relation $J = \rho v$ to calculate the density ρ from the measured flow J and velocity v. The average velocity v is usually overestimated (since standing cars are not detected) and thus the density ρ is underestimated.

The most important empirically measured quantity in traffic flow is the so-called fundamental diagram. It is the relation between the traffic density ρ, measured in vehicles/km, and the traffic flow J, measured in vehicles/hour. Usually the data are averaged over 1 to 5 minute intervals to obtain a time-series of data points. To understand the microscopic structure one needs, however, data which are not averaged and allow to distinguish between the cars (single-vehicle data).

Nowadays one distinguishes three different phases of traffic flow [3]:

- **Free flow:** In the free flow phase the interaction between the vehicles can be neglected. Every car can move with its desired velocity. Therefore the flow increases linearly with the density of cars. The free flow branch F can clearly be seen in Fig. 1. The part of the branch with flows larger than J_{out} is usually called metastable branch for reasons to be discussed later. It corresponds to a region where the flow is not uniquely determined by the density.
  All states not of free flow type are called congested states. Two congested phases can be distinguished.
- **Wide moving jams:** On highways one often observes the so-called stop-and-go traffic, i.e. a sequence of jams. A car leaving one jam soon has to stop due to the next one. Wide (moving) jams are regions with a very high density and negligible average velocity and flow. The width of these structures is much larger than the fronts at its ends where the speed of vehicles changes sharply. Wide jams move upstream [2] with a characteristic velocity v_{Jam}. Empirically one finds $v_{\text{Jam}} \approx 15\ km/h$ [8]. Other characteristic properties of wide jams are its density and the outflow J_{out}, which does not depend on the inflow into the jam. In contrast to synchronized traffic (see below) wide jams can propagate undisturbed through either free flow and synchronized traffic without disturbing these states which thus allows their coexistence. The velocity of the downstream front and the corresponding flow rate is only determined by the density inside a wide jam and the delay-time between two vehicles leaving the jam [8]. In the empirical fundamental diagram in Fig. 1 the wide jams appear on a line with almost no slope. This effect is due to the problems in the density determination from local measurements which lead to an underestimation of the true density (see above).
- **Synchronized flow:** Forms of congested traffic which can not be classified as wide jams constitute synchronized flow [3]. Here the average velocity is significantly lower than in free flow. Nevertheless the flow can be much larger than in wide moving jams. The main characteristic is the apparent absence of a functional flow-density form, i.e. the corresponding data points are spread irregularly over a large two-dimensional area (see Fig. 1). Furthermore, on a multilane highway, the time-series of measurements on different lanes are highly correlated, i.e. synchronized. This was the motivation for denoting this traffic state as "synchronized traffic".

Above we have only given the most important properties of the phases. A more detailed characterization can be found e.g. in [3] (and references therein).

An important quantity (apart from the fundamental diagram) which allows

[2] i.e. opposite to the direction of motion of the vehicles

[3] Actually three different types of synchronized flow can be distinguished, see [3] for details.

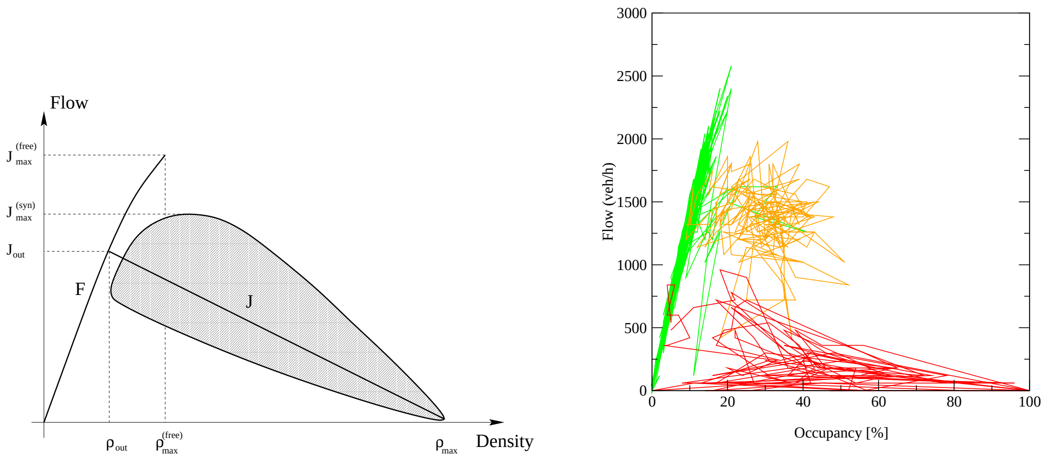

Fig. 1. Left: Schematical form of the fundamental diagram. F denotes the free flow branch and line J is determined by the properties of wide moving jams. Right: Empirical fundamental diagram. One can clearly distinguish the three phases. The differences to the schematical form are mainly due to the use of local measurements for the determination of the empirical fundamental diagram.

to distinguish between the different phases is the cross-correlation [9]

$$cc_{\rho,J}(\tau) = \frac{\langle \rho(t)J(t+\tau)\rangle - \langle \rho(t)\rangle\langle J(t+\tau)\rangle}{\sqrt{\langle \rho^2(t)\rangle - \langle \rho(t)\rangle^2} \cdot \sqrt{\langle J^2(t+\tau)\rangle - \langle J(t+\tau)\rangle^2}} \tag{1}$$

between density ρ and flow J. The autocorrelation of quantities like ρ is then defined as $a_\rho(\tau) = cc_{\rho,\rho}(\tau)$.

The cross-correlation function measures how strong the value of J at time $t+\tau$ depends on the value of ρ at time t. In free flow $cc_{\rho,J}(\tau)$ is very close to 1 [9]. This means that the flow is completely determined by the density. In synchronized flow, on the other hand, the cross-correlation is almost 0 [9]. Here flow and density are independent of each other. This quantifies the earlier statement that the data points are "spread irregularly".

3 Modelling approaches

Very different approaches have been used in order to model traffic flows using methods from physics. There are several ways to distinguish these theories, e.g. macroscopic vs. microscopic, deterministic vs. stochastic, discrete vs. continuous etc. In the following we give a brief (uncomplete) overview over the basic ideas of various popular approaches.

- **Hydrodynamic models**: This approach views traffic as a compressible fluid formed by the vehicles. It is therefore macroscopic and does not distinguish between different cars. Instead the central quantities are densities $\rho(x,t)$ and flows $J(x,t)$ related through a continuity equation $\partial\rho/\partial t + \partial J/\partial x = 0$ which expresses the conservation of the number of vehicles [4]. Since this is only one equation for two unknown functions one needs additional information. Lighthill and Whitham [10] assumed that the flow is completely determined by the density: $J(x,t) = J(\rho(x,t))$. Inserting this relation into the continuity equation yields the so-called Lighthill-Whitham equation

$$\frac{\partial\rho}{\partial t} + v_g\frac{\partial\rho}{\partial x} = 0 \tag{2}$$

with $v_g = dJ/d\rho$. In this approach information about the fundamental diagram $J(\rho)$ has to be provided explicitly. Usually simple forms are used, e.g. $J = \rho v_0(1-\rho/\rho_{\max})$. The solutions of (2) are called kinematic waves. In contrast to dynamic waves these are not determined by a dynamic equation, but only by the conservation of vehicles. Kinematic waves can be interpreted as jam fronts. They are, however, stable objects and can therefore not describe the spontaneous formation of jams.

More realistic approaches interpret traffic as a compressible fluid. Then an additional Navier-Stokes-type equation for the velocity is used which assumes allows for a delay (with some relaxation time τ) of the velocity. A typical form is

$$\frac{\partial v(x,t)}{\partial t} + v\frac{\partial v(x,t)}{\partial x} = -\frac{1}{\rho}\frac{\partial P(x,t)}{\partial x} + \nu(\rho)\frac{\partial^2 v(x,t)}{\partial x^2} + \frac{v_e(\rho) - v(x,t)}{\tau(\rho)}. \tag{3}$$

The first term on the right hand side is usually called traffic pressure with $P(x,t)$ being related to the velocity variance. The viscosity term ν leads to a reduction of spatial inhomogeneities and the last term describes the relaxation to some equilibrium velocity $v_e(\rho)$. In contrast to the Lighthill-Whitham theory this approach shows the existence of unstable and metastable traffic states [11].

- **Gas-kinetic models**: The gas-kinetic approach tries to derive macroscopic models from microscopic equations [12,13]. Traffic is treated as a gas of interacting particles described by a distribution function $P(x,v,t)$ such that $P(x,v,t)dxdv$ is the number of cars at time t which have a position between x and $x+dx$ and a velocity between v and $v+dv$. The time evolution of this distribution function is given by a Boltzmann equation of the form

$$\frac{\partial P}{\partial t} + v\frac{\partial P}{\partial x} = \left(\frac{\partial P}{\partial t}\right)_{\mathrm{rel}} + \left(\frac{\partial P}{\partial t}\right)_{\mathrm{col}}. \tag{4}$$

$\left(\frac{\partial P}{\partial t}\right)_{\mathrm{rel}}$ describes the relaxation of P towards a desired velocity distribution

[4] In the presence of ramps this equation has to be modified by source and sink terms.

$P_{\text{des}}(v)$ in the absence of interactions, e.g.

$$\left(\frac{\partial P}{\partial t}\right)_{\text{rel}} = -\frac{P(x,v,t) - \rho(x,t)P_{\text{des}}(v)}{\tau} \tag{5}$$

where τ is a relaxation time and $P_{\text{des}}(v)$ a desired velocity distribution which has to be determined empirically. The last term $\left(\frac{\partial P}{\partial t}\right)_{\text{col}}$ in equation (4) models the interaction between the vehicles in a similar way as in kinetic gas theory:

$$\begin{aligned}\left(\frac{\partial P}{\partial t}\right)_{\text{col}} &= \int_v^\infty dv'(1 - f_{\text{pass}})(v' - v)P(x,v',t)P(x,v,t)\\ &\quad - \int_0^v dv'(1 - f_{\text{pass}})(v - v')P(x,v,t)P(x,v',t).\end{aligned} \tag{6}$$

This term takes into account that fast cars with velocity v' meet slower one with velocity v at a rate proportional to $P(x,v,t)P(x,v',t)$ and can not overtake these vehicles with probability $1 - f_{\text{pass}}$ thus increasing P. Similarly, P is decreased if vehicles with velocity v can not overtake slower ones with velocity v'.

- **Car-following models**: Car-following theories are microscopic approaches that use ideas from Newtonian mechanics to describe traffic flow. For each car n an equation of motion is given. The acceleration $\dot{v}_n$ is then considered as the reaction to some stimulus. In the simplest form this stimulus is just the velocity difference to the preceeding car [5] :

$$\frac{dv_n(t)}{dt} = \kappa\left[v_{n+1}(t) - v_n(t)\right] \tag{7}$$

The proportionality constant $\kappa > 0$ is usually called sensitivity. (7) has a simple interpretation: If the preceeding car $n+1$ is slower, car n decelerates, if it is faster it accelerates. (7) has been generalized in several ways. E.g. a reaction time T has been introduced by replacing $\frac{dv_n(t)}{dt}$ with $\frac{dv_n(t+T)}{dt}$ in order take into account that a driver does not react instantaneously to a stimulus. This gives rise to stop-and-go waves, but also to the occurance of accidents. Therefore the sensitivity κ is not taken to be a constant, but can itself depend on the spatial headway $\Delta x_n = x_{n+1}(t) - x_n(t)$ or the velocity $v_n(t)$. However, all car-following models suffer from serious problems in the low-density limit. For $\kappa = const.$, the average velocity diverges in the limit $\rho \to 0$. For $\kappa = \kappa(\Delta x_n, v_n)$ the behaviour of free vehicles which have a large distance to the next car ahead is not described realistically.

- **Optimal velocity models**: Optimal velocity models [14] can be considered as a variant of the car-following approach. Here the vehicles do not try to

[5] Throughout the paper we will adopt the convention that cars move from left to right and are numbered in the direction of motion, i.e. car $n+1$ is in front of car n.

adopt the velocity of its predecessor, but an optimal velocity $V_{\rm opt}$ which depends on the headway $\Delta x_n = x_{n+1} - x_n$:

$$\frac{dv_n}{dt}(t) = \frac{1}{\tau}\left[V_{\rm opt}(\Delta x_n) - v_n(t)\right]. \tag{8}$$

In general, $V_{\rm opt}(\Delta x) \to 0$ for $\Delta x \to 0$ in order to avoid accidents. For $\Delta x \to \infty$ cars should not interact. The optimal velocity is bounded by the free flow velocity $v_{\rm max}$, e.g. given by a speed limit, i.e. $V_{\rm opt}(\Delta x \to \infty) = v_{\rm max}$. A typical form is $V_{\rm opt}(\Delta x) \propto \tanh(\Delta x - \Delta x_s) + \tanh(\Delta x_s)$ with some safety distance x_s. Already in this simplest version the optimal velocity model gives quite realistic results compared with empirical data. However, one has to keep in mind that $V_{\rm opt}(\Delta x)$ has to be provided explicitly. Empirically it has been found that the optimal velocity function depends on the traffic state [9]. In addition, since only the acceleration is specified, the model is not automatically collision-free. The so-called intelligent-driver model [15] overcomes these problems by introducing a desired distance function $\Delta x^*(v_n, \Delta v_n)$.

- **Cellular automata**: Cellular automata (CA) are microscopic models which are discrete in space and time and the state variable which in the case of traffic models is usually the velocity. Typically the space discretiziation is chosen in such a way that each cell is occupied by at most one car. Then the length of one cell corresponds to approximately 7.5 m in reality, i.e. the length of a car plus the average headway to the next car in a dense jam.
  The time evolution in CA models is defined through a set of simple rules which contain stochastic elements. Explicit examples will be discussed in Sec. 4 and Secs. 7-9.

4 Cellular automata models

In CA space, time and state variables are discrete which makes them ideally suited for high-performance computer simulations. However, CA modelling differs in several respects from continuum models. These are usually based on differential equations (like (3)) which often can not be treated analytically. One has to solve them numerically and therefore the equations have to be discretized. In general, only space and time variables become discrete whereas the state variable (e.g. the density or velocity in the case of (3)) is still continuous. One important point is now that CA are discrete from the beginning and that this discreteness is already taken into account in the definition of the model and its dynamics. This allows to obtain the desired behaviour in a much simpler way. On the other hand, the numerical solution of (discretized) differential equations is only accurate in the limit Δx, $\Delta t \to 0$. This is different in the CA where Δx and Δt are finite and accurate results can be obtained since the rules (dynamics) are designed such that the discreteness is an important

part of the model.
In order to achieve complex behaviour in a simple fashion one often resorts to a stochastic description. A realistic situation seldomly can be described completely by a deterministic approach. Already minor events can lead to a very different behaviour due to the complexity of the interactions involved. Stochastic components in the description take into account that usually we do not have full knowledge about the systems state and its dynamics. One also has to keep in mind that in general some sort of average over different realizations of the process (e.g. different sequences of random numbers) has to be taken. Even if there are single realizations which yield unrealistic behaviour the average process still can be a good description of the real process.

4.1 The Nagel-Schreckenberg model

The Nagel-Schreckenberg (NaSch) model [16] is a probabilistic cellular automaton able to reproduce many of the basic features of traffic flow discussed in Sec. 2. In the NaSch model the state of each car n ($n = 1, 2, \dots, N$) is characterized by its velocity v_n which can take one of the $v_{max} + 1$ allowed integer values $v = 0, 1, ..., v_{max}$ (see Fig. 2). We denote the position of the n-th

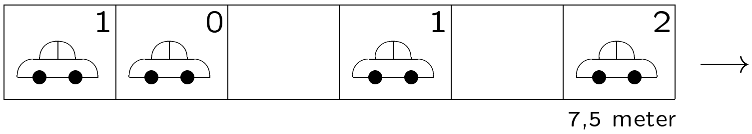

Fig. 2. A typical configuration in the NaSch model. The number in the upper right corner is the speed of the vehicle.

vehicle by x_n. Then $d_n = x_{n+1} - x_n$ is the gap between the n-th car and car $n+1$ in front of it. At each time step $t \to t+1$, the arrangement of the N cars on a finite lattice of length L (i.e. for a global density $\rho = N/L$) is updated *in parallel* according to the following "rules":

Step 1: Acceleration.
If $v_n < v_{max}$, the velocity of the n-th car is increased by one, i.e.

$$v_n \to \min(v_n + 1, v_{max}) \qquad \text{(R1)}.$$

Step 2: Deceleration (due to other cars).
If $d_n \le v_n$, the velocity of the n-th car is reduced to $d_n - 1$, i.e.,

$$v_n \to \min(v_n, d_n - 1) \qquad \text{(R2)}.$$

Step 3: Randomization.

If $v_n > 0$, the velocity of the n-th car is decreased randomly by one unit with probability p, i.e.,

$$v_n \to \max(v_n - 1, 0) \quad \text{with probability } p \qquad \text{(R3)}.$$

Step 4: Vehicle movement.
Each car is moved forward according to its new velocity v_n determined in Steps 1–3, i.e.

$$x_n \to x_n + v_n \qquad \text{(R4)}.$$

All rules have a simple interpretation. *Step 1* expresses the desire of the drivers to move as fast as possible (or allowed). Often $v_{\max}$ corresponds to a speed limit in which case it makes sense that it is the same for all the cars. *Step 2* guarantees the absence of collisions in the model. Note that here the velocity of the preceding car is not taken into account. It turns out that this is already sufficient to reproduce the basic properties of real traffic (see Sec. 4.2). In order to obtain a good agreement with the 'fine-structure' of empirical data a more sophisticated braking rule is necessary. This will be discussed in Sec. 7.

Step 3 looks rather simple but incorporates many effects that play an important role. It introduces an asymmetry between acceleration and deceleration. The acceleration is delayed since a car will accelerate only with probability $1 - p$ if possible. On the other hand, deceleration processes are enhanced. If a car has to brake due to another car ahead (*Step 2*) with probability p it will even brake further in *Step 3*. We will come back to this in Sec. 4.2 since these kind of "overreactions" are the reason for spontaneous jam formation. Another effect incorporated in *Step 3* are natural fluctuations. Even on a free road a driver will not keep a strictly constant velocity which will show small fluctuations.

Finally, in *Step 4* all cars will move with their new velocity which has been determined in the first three steps.

It is worth pointing out that this set of rules is minimal in the sense that every subset of (R1)–(R4) will no longer produce realistic behaviour. E.g. by leaving out (R3) – which is equivalent to the deterministic limit $p = 0$ – one no longer finds spontaneous jam formation (see Sec. 4.2). Also the order of the rules is important. Applying (R2) before (R1) would no longer guarantee the absence of crashes. By interchanging (R2) and (R3), on the other hand, we would no longer observe spontaneous jams [17].

The fundamental diagram of the NaSch model[6] consists of two branches, a free flow and a congested branch, corresponding to the lines F and J in Fig. 1. However, the free flow branch F ends at flow J_{out}, i.e. the NaSch model does not reproduce the metastable states with flow $J_{\text{out}} < J < J_{\text{max}}^{(\text{free})}$. In Sec. 7.1 we will show that already a small modification of the NaSch rules will remedy this problem. Finally, the NaSch model also does not exhibit a synchronized phase. Here larger modifications of the rules are necessary. In Sec. 7.2 we will show that the human desire for comfortable driving plays an important role here. This is not incorporated into the basic NaSch rules which only try to avoid accidents.

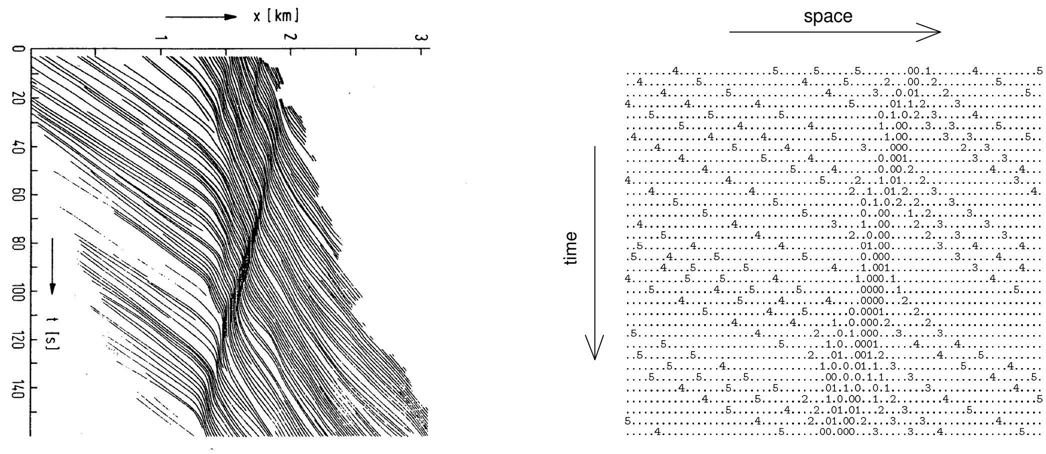

Fig. 3. Trajectories of single cars showing spontaneous jam formation. Left: Empirical data; Right: Computer simulation using the NaSch model. Each number $0, 1, \ldots, v_{\text{max}} = 5$ gives the velocity of the corresponding car.

An important point is the timescale corresponding to one update step. It should not be too small to allow efficient computer simulations, but also not too large.

A simple way to estimate the timescale uses the identification of the maximal velocities. The average velocity of a car not interacting with others is $v_{\text{max}} - p$ and should correspond to a speed limit of e.g. 120 km/h. Taking into account that the length of a cell corresponds to 7.5 m in reality we find

$$\frac{7.5\, m}{\text{cell}} \times \frac{4.5\,\text{cells}}{\text{timestep}} \times \frac{3.6\, sec}{120\, m} \approx 1\ \frac{sec}{\text{timestep}} \tag{9}$$

where we inserted the typical values $v_{\text{max}} = 5$ and $p = 0.5$ used in simulations. This simple estimation shows that one timestep in the simulation corresponds

[6] The fundamental diagram will be discussed in more detail in Sec. 5.

to roughly one second in real time for the chosen parameter values. Since this time is of the same order of magnitude as the smallest relevant timescale in real traffic, namely the reaction time of the drivers, the above parameter values are a reasonable choice.

The NaSch model is also able to reproduce the spontaneous formation of jams (see Fig. 3). It can be understood as an avalanche of overreactions of the drivers. Suppose that a driver has to brake in order to avoid an accident with a slower car in front. Then, with probability p, he will further brake in the randomization step, i.e. he will slow down more than actually necessary to avoid the accident. In a certain density regime this will cause the drivers behind him also to slow down, finally leading to a vehicle with velocity 0 and thus a jam. Fig. 4 shows typical space-time diagrams obtained from simulations of the NaSch model [17]. For the case $p > 0$ one can clearly see various jams with short and long lifetimes. One also recognizes the interesting dynamics of these jams, e.g. their branching behaviour. On the other hand, for the deterministic case $p = 0$, the mechanism described above does not work since overreactions are not possible. Indeed the space-time diagram does not show any jam structures (Fig. 4).

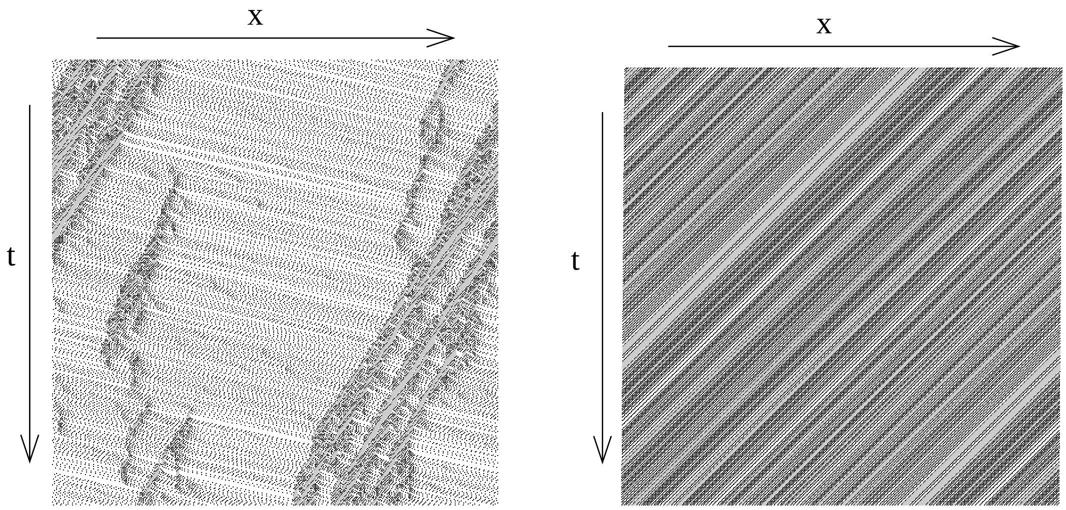

Fig. 4. Typical space-time diagrams of the NaSch model with $v_{max} = 5$ and (a) $p = 0.25, \rho = 0.20$, (b) $p = 0, \rho = 0.5$.

5 Analytical methods

In order to get full information about the time evolution of a stochastic system it is desirable to know $P_{\tau_1,\ldots,\tau_L}(t)$, the probability to find the system at time t in the configuration $(\tau_1, \ldots, \tau_L)$. In our case the variable τ_j characterizes the state of cell j, e.g. $\tau_j = v$, if cell j is occupied by a car with velocity v, and $\tau_j = \times$, if the cell is empty.

The time evolution of $P_{\tau_1,\ldots,\tau_L}(t)$ is determined by the master equation [18] which for stochastic systems with parallel dynamics has the form

$$P_{\tau_1,\ldots,\tau_L}(t+1) = \sum_{\tilde{\tau}_1,\ldots,\tilde{\tau}_L} W(\tilde{\boldsymbol{\tau}} \to \boldsymbol{\tau}) P_{\tilde{\tau}_1,\ldots,\tilde{\tau}_L}(t). \tag{10}$$

In general, the master equation can not be solved exactly, even for the stationary state $P_{\tau_1,\ldots,\tau_L} = \lim_{t\to\infty} P_{\tau_1,\ldots,\tau_L}(t)$.

In this section we give an overview over the different analytical methods which have been used to study the stationary state of the NaSch model. We are looking for exact or approximate solutions of the master equation. This will lead us to a microscopic derivation of different mean-field-type approximations [19–23] which even can become exact in special cases.

5.1 Mean-field theory

We first derive the exact master equation governing the time evolution of $P_{\tau_j}(t)$, the probability to find a cell at time t in state τ_j. The state of cell j at time $t+1$ depends on the states of the $v_{\max}$ cells $j - v_{\max}, \ldots, j-1$ to the left of cell j at time t, from where a car can move into cell j, and on the $v_{\max}$ cells $j+1, \ldots, j+v_{\max}$ to the right, to which a car in cell j could move. The exact master equation for the one-site probabilities thus has the form

$$P_{\tau_j}(t+1) = \sum_{\boldsymbol{\tau}_j^{(2v_{\max}+1)}} W\left(\boldsymbol{\tau}_j^{(2v_{\max}+1)} \to \tau_j\right) P_{\boldsymbol{\tau}_j^{(2v_{\max}+1)}}(t) \tag{11}$$

where $\boldsymbol{\tau}_j^{(2v_{\max}+1)} = (\tau_{j-v_{\max}}(t), \ldots, \tau_{j+v_{\max}}(t))$ is a state of the cluster of $2v_{\max}+1$ cells centered around j and $P_{\boldsymbol{\tau}_j^{(2v_{\max}+1)}}(t)$ the corresponding probability. The transition probabilities $W(\boldsymbol{\tau} \to \tau_j)$ leading from $\boldsymbol{\tau}$ to state τ_j at site j have to be determined from the microscopic rules of the stochastic process.

In the following we will discuss the case $v_{\max} = 1$. Thus we have only to take into account one cell $j-1$ to the left and one cell $j+1$ to the right of j. Fig. 5 shows all 27 possible configurations $(\tau_{j-1}(t), \tau_j(t), \tau_{j+1}(t))$ of the 3-cluster centered around j and the possible new states $\tau_j(t+1)$ at time $t+1$. We have arranged these configurations together with the target states at site j and the corresponding transition probabilities $W(\boldsymbol{\tau}_j^{(3)} \to \tau_j)$ in a table. Note that most configurations appear twice due to the stochastic nature of the rules. E.g. $(\times, 0, \times)$ can lead to $\tau_j(t+1) = 0$ with probability p if the car at site j decelerates in *Step 3* and to $\tau_j(t+1) = \times$ (with probability $1-p$) if it does not decelerate and thus moves to site $j+1$.

Using the table in Fig. 5 we can write down the exact evolution equations by

$\boldsymbol{\tau}_j^{(3)}(t)$	$\tau_j(t+1)$	$W(\boldsymbol{\tau}_j^{(3)} \to \tau_j)$	$\boldsymbol{\tau}_j^{(3)}(t)$	$\tau_j(t+1)$	$W(\boldsymbol{\tau}_j^{(3)} \to \tau_j)$	$\boldsymbol{\tau}_j^{(3)}(t)$	$\tau_j(t+1)$	$W(\boldsymbol{\tau}_j^{(3)} \to \tau_j)$
$\times\times\times$	$\times$	1	$0\ \times\times$	$\times$	p	$1\ \times\times$	$\times$	p
			$0\ \times\times$	1	$1-p$	$1\ \times\times$	1	$1-p$
$\times\times\ v$	$\times$	1	$0\ \times\ v$	$\times$	p	$1\ \times\ v$	$\times$	p
			$0\ \times\ v$	1	$1-p$	$1\ \times\ v$	1	$1-p$
$\times\ v\ \times$	0	p	$0\ v\ \times$	0	p	$1\ v\ \times$	0	p
$\times\ v\ \times$	$\times$	$1-p$	$0\ v\ \times$	$\times$	$1-p$	$1\ v\ \times$	$\times$	$1-p$
$\times\ 0\ v$	0	1	$0\ 0\ v$	0	1	$1\ 0\ v$	0	1
$\times\ 1\ v$	0	1	$0\ 1\ v$	0	1	$1\ 1\ v$	0	1

Fig. 5. Configurations $\boldsymbol{\tau}_j^{(3)}(t) = (\tau_{j-1}(t), \tau_j(t), \tau_{j+1}(t))$ of a 3-cluster at time t and possible transitions. $\times$ denotes an empty cell, 0 (1) a cell occupied by a car with velocity 0 (1) and v stands for a cell occupied by a car with velocity $v = 0, 1$. Also given are the transition probabilities $W(\boldsymbol{\tau}_j^{(3)} \to \tau_j)$.

summing over all configurations leading to the same $\tau_j(t+1)$. Gathering all configurations $\boldsymbol{\tau}_j^{(3)}(t)$ that lead to $\tau_j(t+1) = 1$ yields

$$\begin{aligned} P_1(t+1) &= (1-p)\left[P_{0\times\times}(t) + P_{1\times\times}(t) + \sum_{v=0}^{1} P_{0\times v}(t) + \sum_{v=0}^{1} P_{1\times v}(t)\right] \\ &= (1-p)\left[P_{0\times}(t) + P_{1\times}(t)\right] = (1-p)\sum_{v=0}^{1} P_{v\times}(t). \end{aligned} \tag{12}$$

Here we have used the so-called Kolmogorov consistency conditions [24]

$$\sum_{\tau} P_{\tau_1,\ldots,\tau_{n-1},\tau}(t) = P_{\tau_1,\ldots,\tau_{n-1}}(t) = \sum_{\tau} P_{\tau,\tau_1,\ldots,\tau_{n-1}}(t) \tag{13}$$

where the summation runs over all allowed values $\tau = \times, 0, 1, \ldots, v_{\max}$. The Kolmogorov conditions hold for any cluster size n. They relate n-cluster probabilities with those of an $(n-1)$-cluster and follow from the normalization of the probabilities.

Similarly we get for $\tau_j(t+1) = 0$ and $\tau_j(t+1) = \times$, respectively,

$$P_0(t+1) = \sum_{v,\tilde{v}=0}^{1} P_{v\tilde{v}}(t) + p\sum_{v=0}^{1} P_{v\times}(t), \tag{14}$$

$$P_\times(t+1) = P_{\times\times}(t) + \sum_{v=0}^{1} P_{v\times}(t) = P_\times(t), \tag{15}$$

where we have already used (13) to simplify the equations.

The equations (12-15) are exact. We see, however, that the time evolution is determined by the 2- and 3-cluster probabilities. When we try to determine these higher cluster probabilities we will see that we need to know the time evolution of even larger clusters. In order to get a solvable set of equations we have to close the system by approximating large clusters through small ones. The mean-field approximation (MFA) is obtained if we replace in (12), (14), (15) all probabilities 2-cluster through 1-cluster probabilites, i.e. assuming

$$P_{\tau\tilde{\tau}}(t) \approx P_{\tau}(t) P_{\tilde{\tau}}(t). \tag{16}$$

This implies that all correlations between neighbouring cells are completely neglected. Then (12-15) becomes a nonlinear system of equations for the single-site probabilities $P_\tau(t)$ only. Since we are mainly interested in the properties of the stationary state reached after a long time we can replace $P_\tau(t)$ and $P_\tau(t+1)$ by the stationary values $P_\tau = \lim_{t\to\infty} P_\tau(t)$. Then we obtain the stationary mean-field equations

$$P_1 = (1-p)\sum_{v=0}^{1} P_v P_\times = (1-p)(1-P_\times)P_\times = (1-p)\rho(1-\rho), \tag{17}$$

$$P_0 = \rho(\rho + p(1-\rho)) \tag{18}$$

where we have used the normalization $P_\times + P_0 + P_1 = 1$ and $P_0 + P_1 = \rho$. This implies $P_\times = 1 - P_0 - P_1 = 1 - \rho$, as expected.

The above calculations can be simplified slightly by writing down the master equation after the first step of the update. This is equivalent to using the update-ordering R2-R3-R4-R1 instead of R1-R2-R3-R4. Since after the acceleration step there are no cars with velocity 0 this reduces the number of states per cell by one ($\tau_j = \times, 1, ..., v_{\max}$). For $v_{\max} = 1$ we then do no longer distinguish between moving and standing cars, i.e. we are using occupation numbers n_j, where $n_j = 0$ denotes an empty cell and $n_j = 1$ an occupied one. The change of the ordering reduces the number of evolution equations by one and has to be taken into account in the calculation of observables. In the occupation number representation we will use a slightly different notation as a reminder of the different update-ordering and write $P(n_1, \dots, n_n)$ instead of $P_{\tau_1,\dots,\tau_n}$ for the n-cluster probabilities.

If one uses the changed update-ordering R2-R3-R4-R1 the probability $P(n_1, \dots, n_L)$ to find the system in the state $(n_1, \dots, n_L)$ is given by

$$P(n_1, \dots, n_L) = \prod_{j=1}^{L} P(n_j) = (P(0))^{L-N}(P(1))^N. \tag{19}$$

(19) implies that in the stationary state of mean-field type for fixed number N of particles all configurations appear with the same probability.

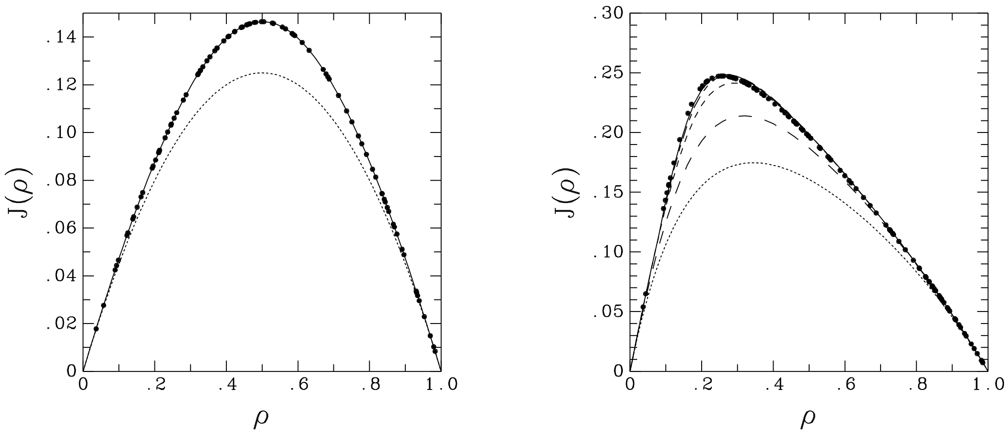

Fig. 6. Fundamental diagram of the NaSch model for different $v_{\max}$. The dots represent the results of Monte Carlo simulations. a) $v_{\max} = 1$: The full line is the 2-cluster approximation and the dotted line the mean-field result. b) $v_{\max} = 2$: The lines correspond to the results of the n-cluster approximation for $n = 1, 2, \ldots, 5$ (from bottom to top).

Fig. 6 shows that the mean-field result considerably underestimates the flow. This implies that correlations play an important role. These correlations can be characterized by a particle-hole attraction, i.e. the probability to find an empty cell ('hole') in front of an occupied cell ('particle') is enhanced compared to a completely random distribution of particles and holes (as assumed in the mean-field approach). More explicitly the particle-hole attraction implies $(P_0 + P_1)P_\times = \rho(1-\rho) \leq P_{0\times} + P_{1\times}$ or, in the occupation number representation,

$$P(0)P(1) = (1-\rho)\rho \leq P(0,1). \tag{20}$$

Note that the fundamental diagram for $v_{\max} = 1$ is symmetric with respect to $\rho = 1/2$. This is due to a particle-hole symmetry, i.e. a particle moving to the right means a hole moving to the left.

It is surprising that for random-sequential dynamics the MF approximation is exact for $v_{\max} = 1$ [16]. In random-sequential dynamics the update rules are not applied to all particles synchronously, but in each timestep a cell which is updated is picked at random. Since MF is exact there is no particle-hole attraction for random-sequential dynamics. In Sec. 5.2 we will see how this difference to the parallel update can be understood.

For $v_{\max} > 1$ the system is no longer particle-hole symmetric and the fundamental diagram becomes more realistic, i.e. the maximum is shifted to smaller densities. The mean-field calculations can also be extended to the case $v_{\max} > 1$ [20]. One finds a qualitatively similar behaviour, i.e. the particle-hole attraction exists for all velocities (Fig. 6).

One may wonder why we have not used the update-ordering R2-R3-R4-R1 to simplify the mean-field calculations of Sec. 5.1. In this section we will show that the results in the original formulation with the ordering R1-R2-R3-R4 can be extended to obtain better or even exact results. Furthermore we will get some understanding where the differences between the random-sequential and parallel updates mentioned at the end of the previous section come from.

An important effect of the parallel dynamics is the existence of configurations which can not be reached dynamically [22]. These states are called Garden of Eden (GoE) states or paradisical states since one never gets back once one has left [25]. An example for a GoE state is given in Fig. 7. Note that the velocity is equal to the number of cells that the car moved in the previous timestep. For the configuration shown in Fig. 7 this implies that the two cars must have occupied the same cell before the last timestep. Since this is forbidden in the NaSch model, the configuration shown can never be generated by the dynamics.

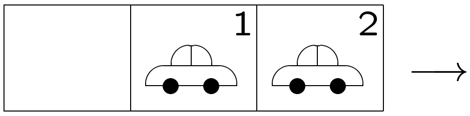

Fig. 7. A Garden of Eden state for the NaSch model with $v_{\max} \geq 2$.

The simple mean-field theory presented in the previous section does not take into account the existence of GoE states. One can therefore hope that by eliminating all GoE states and applying mean-field theory in the reduced configuration space (paradisical mean-field, pMF) one will find a considerable improvement of the MF results.

For $v_{\max} = 1$ all states containing the local configurations $(0,1)$ or $(1,1)$ are GoE states, i.e. the cell behind a car with velocity 1 must be empty [7]. We therefore have to eliminate all GoE states contributing to the MF equations (12),(14) and (15). Since $P_\times(t) = 1-\rho$ gives the (conserved!) number of empty cells the corresponding equation is again satisfied automatically and need not to be considered here. It turns out that no GoE states contribute to $P_1(t+1)$, but only to $P_0(t+1)$. In the first term of (14), $P_{01}(t)$ and $P_{11}(t)$ are GoE states. Instead of (12) and (14) we find after elimination of these states

[7] Here we use the original update ordering, so '0' denotes a cell occupied by a car with velocity 0.

$$P_1(t+1) = \mathcal{N}(1-p)\sum_{v=0}^{1} P_{v\times}(t), \tag{21}$$

$$P_0(t+1) = \mathcal{N}\left[P_{00}(t) + P_{10}(t) + p\sum_{v=0}^{1} P_{\times v}(t)\right]. \tag{22}$$

Note that we have to introduce a normalization $\mathcal{N}$ to ensure $P_0 + P_1 = \rho$. It takes into account the reduction of the configuration space due to the elimination of the GoE states.

Assuming factorization of the 2-cluster probabilities we obtain the equations for the paradisical mean-field (pMF) theory:

$$P_0 = \mathcal{N}(P_0 + p(1-\rho))\rho\ , \tag{23}$$
$$P_1 = \mathcal{N}(1-p)\rho(1-\rho)\ , \tag{24}$$

with $\mathcal{N} = 1/(P_0 + 1 - \rho)$.

For $v_{\max} = 1$ the flow is simply given by the number of moving cars, i.e. $J(\rho) = P_1$. Solving (24) for P_1 by using $P_0 = \rho - P_1$, one obtains P_1 as a function of the density ρ and thus

$$J(\rho) = \frac{1}{2}\left(1 - \sqrt{1 - 4(1-p)(1-\rho)\rho}\right). \tag{25}$$

We will see in Section 5.3 that this result is indeed exact!

We have already pointed out that for random-sequential dynamics MF theory is exact. In contrast, for parallel dynamics pMF is exact. Therefore the origin of the correlations is the parallel update procedure. The existence of the GoE states is responsible for the differences between parallel and random-sequential dynamics. This is probably not only true for the NaSch model, but is a rather general property of CA models.

For $v_{\max} = 2$ one has to take into account more GoE states [22]. pMF is no longer exact, but it still leads to a considerable improvement of the MF results. This implies a qualitative difference to the case $v_{\max} = 1$ where all correlations are a consequence of the existence of GoE states. For $v_{\max} > 1$, however, "true" correlations exist.

5.3 Cluster approximation

In Subsection 5.1 we have explained the microscopic derivation of the mean-field equations in a rather formal manner. Of course they can be derived in a much more intuitive way, too. However, the technique explained in Sec. 5.1 can straightforwardly be generalized to the so-called cluster approximation [19,20]. The latter is a systematic improvement of MF theory which takes into account short-ranged correlations between the cells. In the n-cluster approximation a cluster of n neighbouring cells is treated exactly. Each cluster is coupled to the rest of the system in a self-consistent way. The MF theory of Sec. 5.1 then corresponds to the 1-cluster approximation.

For a 2−cluster of consecutive cells with state variable $\boldsymbol{\tau}_j^{(2)}(t) = (\tau_j(t), \tau_{j+1}(t))$ at time t it is straightforward to derive an exact evolution equation for the cluster probability $P_{\tau_j(t),\tau_{j+1}(t)}$ by generalizing the calculations of Sec. 5.1. E.g. for the 2-cluster approximation in the case of $v_{\max} = 1$ one obtains equations which express $P_{\tau_j,\tau_{j+1}}$ through 4-cluster probabilities $P_{\tau_{j-1},\tau_j,\tau_{j+1},\tau_{j+2}}$. In order to obtain a closed set of equations an approximation has to be made in order to express the 4-cluster through the 2-cluster probabilities. Similar to the factorization (16) used in the MFT one now uses (see Fig. 8)

$$P(\boldsymbol{\tau}^{(4)}) \approx P(\tau_{j-1}|\underline{\tau_j}) \cdot P(\tau_j, \tau_{j+1}) \cdot P(\underline{\tau_{j+1}}|\tau_{j+2}) \tag{26}$$

with the conditional probabilities

$$P(\tau_1|\underline{\tau_2}) = \frac{P(\tau_1, \tau_2)}{\sum_\tau P(\tau, \tau_2)}, \qquad P(\underline{\tau_1}|\tau_2) = \frac{P(\tau_1, \tau_2)}{\sum_\tau P(\tau_1, \tau)} \ . \tag{27}$$

In this way we obtain an nonlinear system of equations for the 2-cluster probabilities which can be solved analytically in the case $v_{\max} = 1$ and yields [19,20]

$$\begin{aligned} P(0,0) &= 1 - \rho - P(1,0) \ , \\ P(1,1) &= \rho - P(1,0) \ , \\ P(1,0) &= P(0,1) = \frac{1}{2(1-p)} \left[1 - \sqrt{1 - 4(1-p)\rho(1-\rho)}\right] \ , \end{aligned} \tag{28}$$

where we have used the ordering R2-R3-R4-R1. The flow is given by $J(\rho) = (1-p)P(1,0)$ which yields again (25).

These calculations can further be generalized by taking into account even more short-ranged correlations. Surprisingly for $v_{\max} = 1$ the results for the n-cluster approximation turn out to be identical for $n \geq 2$ [19]. This indicates that the 2-cluster result is exact which indeed can be shown to be true, e.g. by using combinatorial arguments [20].

In general, the master equation in n-cluster approximation leads to $(v_{\max}+1)^n$ nonlinear equations. This number can be reduced by using the Kolmogorov

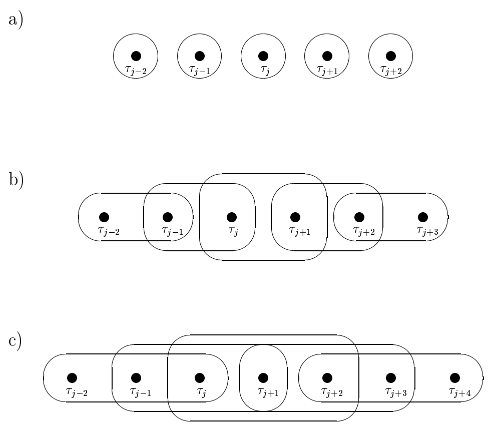

Fig. 8. Graphical representation of the factorization into clusters in the $n-$cluster approximation for a) $n = 1$ (i.e. mean-field theory), b) $n = 2$, and c) $n = 3$.

consistency conditions (13). Nevertheless, a solution is only feasible for relatively small cluster-sizes [20]. The quality of the approximation improves with increasing n and for $n \to \infty$ the n-cluster result becomes exact.

For $v_{\max} = 2$ the results for the fundamental diagram obtain from the n-cluster approximation are shown in Fig. 6. Already for $n = 4$ the agreement with Monte Carlo simulations is excellent.

5.4 Car-oriented mean-field

The car-oriented mean-field (COMF) theory [21] is another possibility to take into account correlations in an analytical description.

The rules R1–R4 can be rewritten in terms of the headway d_j and the velocity v_j only. Therefore the state of the system can be characterized equivalently by the headways and the velocities [8] instead of the states τ_j. This can be used also in Monte Carlo simulations to make them at low densities more efficient [20]. The central quantity in COMF is the probability $D_n(v)$ to find exactly n empty cells (i.e. a gap of size n) in front of a car with velocity v. In this way certain longer-ranged correlations are already taken into account. The essence of COMF is now to neglect correlations between the headways.

In the following we treat the case $v_{\max} = 1$ and use the update ordering R2-R3-R4-R1 (see Sec. 5.3). Since all vehicles have $v_j = 1$ after *Step 1* we can drop the velocity dependence of $D_n(v)$. The probabilities D_n (with $D_n = D_n(v = 1)$) have to satisy the normalization conditions

[8] For a complete equivalence one has to track the position x_1 of one car, e.g. car 1. From x_1 one can then determine $\{\tau_j\}$ if all headways and velocities are known.

$$1 = \sum_{n=0}^{\infty} D_n \qquad \text{and} \qquad \frac{1}{\rho} = \sum_{n=0}^{\infty} (n+1) D_n \ . \tag{29}$$

The second identity is a consequence of the conservation of the number of cars since each car with headway n occupies $n+1$ cells.

In the stationary state one obtains the following system of equations from the master equation:

$$\begin{aligned}
D_0 &= \bar{g}\left[D_0 + (1-p)D_1\right] \ , \\
D_1 &= g D_0 + \left[(1-p)g + p\bar{g}\right] D_1 + (1-p)\bar{g} D_2 \ , \\
D_n &= p g D_{n-1} + \left[(1-p)g + p\bar{g}\right] D_n + (1-p)\bar{g} D_{n+1} \ , \quad (n \geq 2)
\end{aligned} \tag{30}$$

where $g = (1-p)\sum_{n\geq 1} D_n = (1-p)[1-D_0]$ is the probability that a car moves in the next timestep. $\bar{g} = 1-g$ then is the probability that a car does not move.

As an example for the derivation of (30) we consider the equations for $n \geq 2$. Since the velocity difference of two cars is at most 1, a gap of n cells at time $t+1$ must have evolved form a gap of length $n-1$, n, or $n+1$ in the previous timestep. A headway of $n-1$ cells evolves into a headway of n cells only if the first car moves (with probability g) and the second car brakes in the randomization step (probability p), i.e. the total probability for this process is pgD_{n-1}. Similarly, the headway remains constant only if either both cars move (probability $(1-p)g$) or both cars do not move (probability $p\bar{g}$). Finally, the headway is reduced by one, if only the second car moves (probability $(1-p)\bar{g}$).

Although the infinite system of non-linear equations (30) looks more difficult than those of the cluster approximation, a solution possible using generating functions [21]. For $v_{\max} = 1$ one finds

$$\begin{aligned}
D_0 &= \frac{1}{2(1-p)\rho}\left[2(1-p)\rho - 1 + \sqrt{1-4(1-p)\rho(1-\rho)}\right] \ , \\
D_n &= \frac{D_0}{p}\left(\frac{p(1-D_0)}{D_0 + p(1-D_0)}\right)^n \qquad (n \geq 1),
\end{aligned} \tag{31}$$

and for the flow $J(\rho, p) = \rho g$ again the exact solution (25) is reproduced.

For $v_{\max} = 2$ one has two coupled systems of the type (30), since one has to distinguish $D_n(v=1)$ and $D_n(v=2)$ and the probabilities g_α that a car moves $\alpha = 0, 1, 2$ cells in the next timestep. This system has a similar structure as (30) and is given explicitly in [21]. It can also be solved, but does not give the exact solution. The results for the fundamental diagram are comparable to those of the 3-cluster approach.

6 Nonequilibrium effects and phase transitions

Traffic flow models are not only interesting for practical applications, but also allow to study interesting physics. The CA models, which are at the center of this review, are systems far from equilibrium. In such nonequilibrium systems many fascinating effects can be observed. We will discuss only a few examples here. For a more detail investigation of nonequilibrium physics and some of the topics of this Section we refer to the lectures by M.R. Evans [18]. There also several other reviews and books [26–28] which cover the topics discussed here.

6.1 Open boundary conditions

So far we have only considered periodic boundary conditions. The main reasons are that then the number of cars is constant and the stationary state is translational invariant. There are, however, situations where other boundary conditions are more appropriate, e.g. for the so-called bottleneck situation. A simple example is a two-lane road where one lane is blocked in a certain region, e.g. due to road construction. A simple model for this one-lane stretch of the road is a NaSch model with open boundary conditions. The two-lane parts of the road are then assumed to constitute "reservoirs" of density ρ_L and ρ_R (see Fig. 9), respectively, from which cars enter or to which cars exit. Often one uses probabilities α, β instead of the densities ρ_L and ρ_R. α is then the probability that a car enters and β the probability that a car leaves.

For the case $v_{\max} = 1$ this model has been studied for a long time in many different contexts. It is then called the Asymmetric Simple Exclusion Process (ASEP). One can see the reason for this name if one reformulates the dynamics slightly. In this case a car (or particle) hops to its right neighbour cell with probability $1 - p$ if this cell is empty. "Simple Exclusion" then refers to the absence of multiply occupied cells and "Asymmetric" to the fact that a motion is only allowed in one direction.

The ASEP has been studied extensively in recent years and is now well understood (see e.g. [18,28] and references therein). In fact its stationary state for different dynamics can be obtained exactly. It shows an interesting phase diagram (see Fig. 9) and is the prototype for so-called boundary-induced phase transitions.

Fig. 9 shows the generic form of the phase diagram obtained by varying the boundary rates α and β in a NaSch model with $v_{\max} = 1$. One can distinguish three phase, namely (A) a low-density phase, (B) a high-density phase and (C) a maximal-current phase. The appearance of these three phases can easily

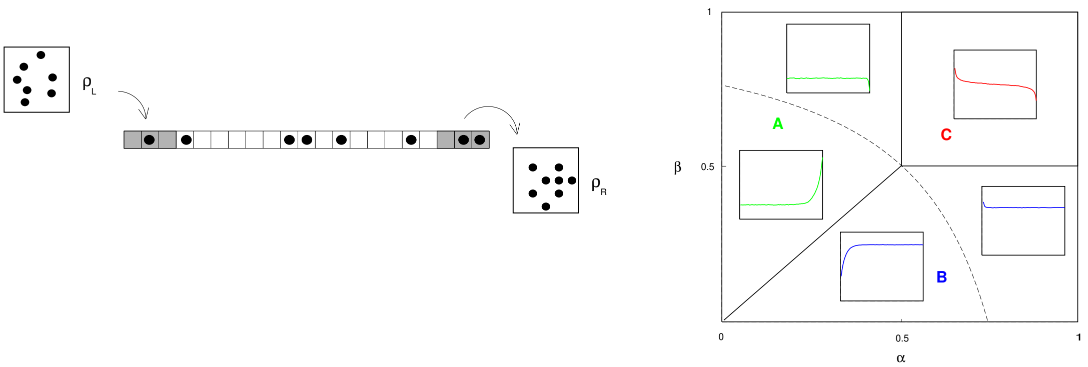

Fig. 9. NaSch model with open boundary conditions (left); Phase diagram of the ASEP (right). The insets show the typical shape of the density profiles in the corresponding region.

be understood. In the low-density phase the current dependents only on the input rate α. The input is less efficient than the transport in the bulk of the system or the output and therefore dominates the behaviour of the whole system. In the high-density phase the output is the least efficient part of the system. Therefore the current depends only on β. In the maximal current phase, input and output are more efficient than the transport in the bulk of the system. Here the current has reached the largest possible value corresponding to the maximum of the fundamental diagram of the periodic system. The phase diagrams for NaSch models with $v_{\max} > 1$ look qualitatively the same.

A nice physical picture which also allows for quantitative predictions for the phase diagram has been developed in [29]. It relates the phase boundaries to properties of the periodic system which can be derived from the fundamental diagram, namely the so-called shock velocity $v_s = \frac{J(\rho^+)-J(\rho^-)}{\rho^+-\rho^-}$ and the collective velocity $v_c = \frac{\partial J(\rho)}{\partial \rho}$. v_s is the velocity of a 'domain-wall' which in nonequilibrium systems denotes an object connecting two possible stationary states. Here these stationary states have densities ρ^+ and ρ^-, respectively. The collective velocity v_c describes the velocity of the center-of-mass of a local perturbation in a homogeneous, stationary background of density ρ.

The results for the ASEP show that boundary conditions play an important role in nonequilibrium systems. For most traffic applications periodic boundary conditions are not very realistic. Here the number of vehicles is conserved whereas in real traffic it fluctuates strongly, e.g. due to on- and off-ramps. In [30,31] the results for open systems like the ASEP have indeed been used for the interpretation of empirical traffic data. In that case these data provided the first direct observation of a boundary-induced phase transition of first order.

So far we have not considered the effects of disorder on the behaviour of the NaSch model. All vehicles had the same properties, i.e. $v_{\max}$ and p. In real traffic, this is in general not true. Therefore it is important to study the effects of disorder. Two types can be distinguished, particlewise and sitewise disorder [32]. In a model where a finite number (in the thermodynamic limit) of particles (vehicles) or sites has different properties from the rest these are usually called *defects*. In the first case, corresponding to a limiting case of particlewise disorder [33–36], the defect particles may have a smaller maximal velocity. Such defects are not localized in space in contrast to those corresponding to sitewise disorder where in a localized region certain parameters of the model take different values, e.g. by imposing a speed limit or increasing the decelaration probabilities [37–44].

In both cases a parameter regime exists where the global behaviour of the system is controlled by the defect which acts as a bottleneck. Generically it induces phase separation into a high and a low density region separated by a sharp discontinuity ("shock"). In the case of particlewise disorder with one slow car (and no overtaking) the faster cars tend to pile up behind the slow one. This behaviour has certain similarities with Bose-Einstein condensation [33,34]. For a spatially localized defect one also finds a separation into a high and a low density regime, but with the high density region pinned to the defect. This behaviour has been found in a variety of models and for different defect realizations.

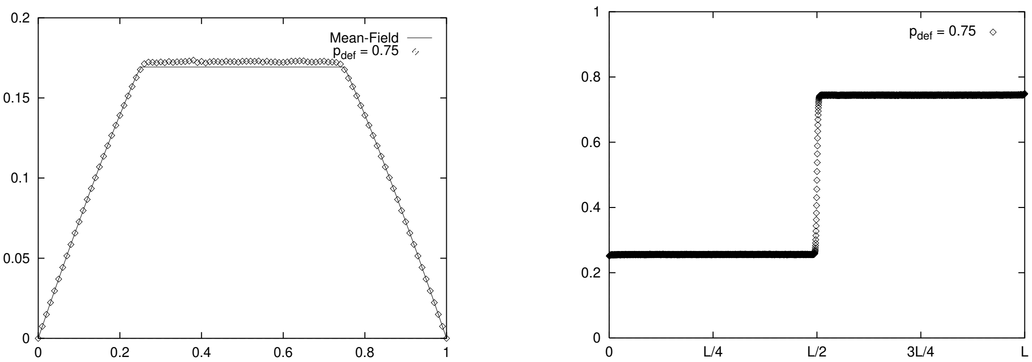

Fig. 10. The NaSch model ($v_{\max} = 1$) with a defect site at $j = 0$. Left: Fundamental diagram; Right: Density profile (with shock).

6.3 Phase transition

Many interesting problems in statistical physics are connected with phase transitions. In the previous two subsection we have already presented examples for nonequilibrium phase transitions in variants of the NaSch model. Now we want to discuss briefly the question whether the NaSch model itself exhibits a phase transition between free flow and congested flow.

In the deterministic case $p = 0$ the situation is rather clear. Here the flow is given by $J(\rho) = \min(\rho\, v_{\max}, 1 - \rho)$. Below the critical density

$$\rho_{\text{crit}} = \frac{1}{v_{\max} + 1} \tag{32}$$

the cars can arrange in such a way that every vehicle has at least $v_{\max}$ empty cells in front and can thus move with velocity $v_{\max}$. This is no longer possible for $\rho > \rho_{\text{crit}}$. Thus at the density ρ_{crit} one finds a second order phase transition from the free flow to a jammed phase. A suitable order parameter for the description of this transition is the density of nearest neighbour pairs [45]

$$m = \frac{1}{L} \sum_{j=1}^{L} n_j n_{j+1}, \tag{33}$$

with $n_j = 0$ for an empty cell and $n_j = 1$ for a cell occupied by a car (irrespective of its velocity). $m > 0$ for all densities above ρ_{crit} and vanishes continuously at the critical density.

In the presence of noise ($p \neq 0$) the behavior of the order parameter qualitativly changes in the vicinity of the transition density. Within this region m decays exponentially as a function of ρ. It does not exhibit a sharp transition. Although it becomes rather small for small densities it is still different from zero. The situation is quite similar to the behavior of the order parameter in finite systems. The transition is smeared out by the noise and the transition density is shifted towards smaller values. This behaviour indicates that there is no critical point for $p \neq 0$, but just a crossover. There are further indications for this scenario, e.g. the existence of a cutoff in the lifetime distribution of jams [46]. Spatial correlations do not show algebraic decay [45] and especially the density-density correlations decay exponentially for all densities. The maximal correlation length diverges only in the limit $p \to 0$ [45,23]. This is consistent with the existence of a critical point at density ρ_{crit} in the deterministic case $p = 0$. For $p > 0$ also the distribution of jam sizes shows an exponential behavior. Therefore one does not find any indication of critical behavior in the spatial direction in this case. Only the dynamical structure factor shows features which might be interpreted as indication for critical behaviour [47]. However, these results are still consistent with the above scenario since the system sizes and simulation times for the calculation of structure factors are too small to see e.g. the cutoff in the lifetime distribution of jams [48].

7 Improved cellular automata models

In Sec. 4 we have seen that the NaSch model reproduces the basic structure of the fundamental diagram and the appearance of spontaneous jam formation. However, it is does not exhibit metastable states of high flow and sychronized traffic. In the following we will describe two variants of the basic NaSch model which are able to solve these problems.

7.1 VDR model

In order to reproduce the metastable states of high flow corresponding to states with $J > J_{\rm out}$ on the free flow branch F in Fig. 1 only a simple modification of the NaSch model is necessary. This leads to the so-called Velocity-Dependent-Randomization (VDR) model [49]. Here, in contrast to the original NaSch model, the randomization parameter depends on the velocity of the car, $p = p(v)$. The rules of Sec. 4.1 are supplemented by a new rule,

Step 0: Determination of the randomization parameter.
The randomization parameter used in *Step 3* for the n-th car is given by $p = p(v_n(t))$.

This new step has to be carried out before the acceleration *Step 1*. The randomization parameter used in *Step 3* depends on the velocity $v_n(t)$ of the $n-$th car after the previous timestep. Metastable states occur for so-called slow-to-start rules where one chooses [49]

$$p(v) = \begin{cases} p_0 & \text{for } v = 0, \\ p & \text{for } v > 0, \end{cases} \tag{34}$$

with $p_0 > p$. This means that cars which have been standing in the previous timestep have a higher probability p_0 of braking in the randomization step than moving cars, explaining the name 'slow-to-start' rule.

Fundamental diagrams obtained from Monte Carlo simulations of the VDR model consist of the two branches F and J in Fig. 1, including the states with $J > J_{\rm out}$. However, no synchronized traffic is found in this simple modification.

The macroscopic structure of the congested sate in the VDR model is very different from that of the NaSch model [17,49]. It exhibits phase separation into a free flow region and a large jam which is almost compact for $p \ll 1$ (see Fig. 11). In contrast, in the original NaSch model stop-and-go waves are found (see Fig. 4). On the other hand, the structure of the free flow branch is very similar to that of the NaSch model. However, for $J > J_{\rm out}$ the homogeneous free flow states are not stable, but can decay to a congested state through fluctuations or small perturbations (see Fig. 11).

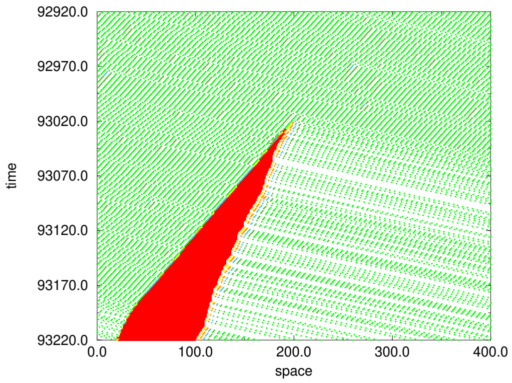

Fig. 11. Typical space-time diagram of the VDR model with $v_{\max} = 5$ and $\rho = 0.20$, $p = 0.01$ and $p_0 = 0.75$. One can clearly see the formation of a large compact jam. The diagram should be compared with that for the NaSch model (Fig. 4).

The fundamental diagram of the VDR model can be understood from heuristic arguments utilizing the observed structures of the steady-states. For small densities $\rho \ll 1$ there are no slow cars in the VDR model since interactions between cars are extremely rare. Every car moves with the free-flow velocity $v_f = v_{\max} - p$ and, therefore, the flux is given by

$$J_{\text{hom}}(\rho) = \rho(v_{\max} - p) \tag{35}$$

which is identical to the NaSch model with randomization p. On the other hand, for densities close to $\rho = 1$, the cars are likely to have velocities $v = 0$ or $v = 1$ only and, therefore, the random braking is dominated by p_0. A simple waiting time argument [49] shows that the flow in the phase-separated regime is given by

$$J_{\text{sep}}(\rho) = (1 - p_0)(1 - \rho). \tag{36}$$

This corresponds to the free flow branch of a NaSch model with randomization p_0.

The behaviour found in the VDR model is generic for models with slow-to-start rules. Due to the slow-to-start rule the outflow from a large jam is smaller than the maximal possible flow, i.e. the maximum of the fundamental diagram. Note that the large jam is only stable if the outflow J_{out} equals the inflow J_{in}. For $J_{\text{out}} = J_{\max}^{(\text{free})}$ it is very unlikely that this condition can be satisfied. Therefore the density far downstream is rather small, which can clearly be observed in Fig. 11, and the vehicles propagate almost freely in the low-density region. The spontaneous formation of jams is suppressed if p is not too large. This is the basic mechanism which leads to the formation of the phase-separated state and hysteresis.

Although the VDR model shows metastable states and related phenomena like hysteresis it is not able to reproduce the characteristic properties of synchronized traffic and the agreement with empirical data on a microscopic level is not very satisfactory. This indicates that an important ingredient is still missing. So far the dynamics of all CA models that we have discussed were mainly based on the avoidance of accidents. This appears to be insufficient. Therefore it has been suggested that the desire of the drivers for smooth and comfortable driving is responsible for the occurrence of synchronized traffic in highway traffic [50]. The avoidance of accidents implies that only interactions with the next car ahead are important. So far we have not taken into account any information about the velocity or the velocity difference to the preceeding car. As we know from our own experience usually one tries to "anticipate" the behaviour of the predecessor. E.g. if its headway is rather large than we know that it is very unlikely that he will brake abruptly. Therefore we are willing to accept a much smaller headway than in denser traffic. Thus anticipation allows for a much smoother driving.

The following aspects appear to be important:
(i) Velocity anticipation: At inhomogeneities, e.g. created by ramps, the anticipation of the leaders velocity avoids abrupt braking of the traffic behind and therefore reduces the probability to form jams.
(ii) Retarded acceleration: Comfortable driving also implies that cars do not accelerate immediately in case of a larger gap ahead if they observe slow downstream traffic. On the one hand, this leads in some sense to a sub optimal gap usage, because the velocity is smaller than the headway allows. On the other hand, larger gaps in a dense region reduce the car-car interactions what may cut a chain of braking overreactions which is responsible for the formation of jams. These overreactions are a direct consequence of the delayed human behavior in adapting the velocity to the headway which can lead to an avalanche like amplification of the velocity fluctuations upstream and finally to the formation of jams.
(iii) Timely braking: Finally timely braking suppresses another mechanism of jam formation: When the velocity adjustment is only based on the distance to the next car ahead, jams often emerge in the layer between free-flow and synchronized traffic. In these models the jam formation arises from cars approaching a slow-moving cluster with high speed which leads to a compactified region. In contrast, our approach avoids this artificial mechanism to form a jam, the drivers adjust their speed to the vehicles ahead.

An important feature for realizing (i)–(iii) is the possibility to anticipate the actions of other cars in the next timestep. This implies that drivers need more information about the next car $n+1$ ahead, not just its distance d_n as in the NaSch model. E.g. by knowing its velocity $v_{n+1}(t)$ and headway $d_{n+1}(t)$ it is clear that $v_n(t+1) \geq v_{\rm anti}$, where $v_{\rm anti} = \min(d_{n+1}(t), v_{n+1}(t))$ is the anticipated velocity of the preceeding car, will be a safe velocity not leading to a collision.

Based on these aspects a new CA model has been suggested in [51]. The rules are more complex than for the VDR model. Apart from a slow-to-start rule like in the VDR model it incorporates anticipation through the introduction of an interaction horizon and brake lights which indicate velocity changes of the preceeding car. Another feature is a reduced cell length of 1.5 m instead of 7.5 m as in the standard NaSch model. Therefore the vehicles now have a length of 5 cells. This allows for a smoother acceleration and deceleration.

These refinements of the model lead to the following characteristics of the drivers' behaviour which appear to be important for synchronized traffic:
(i) For large headways cars move, apart from fluctuations, with their desired velocity $v_{\rm max}$.
(ii) For intermediate headways drivers react to velocity changes of the next vehicle downstream. This is implemented by introducing brake lights.
(iii) For small headways drivers adjust their velocity such that safe driving is possible.
(iv) The acceleration is delayed for standing vehicles (slow-to-start) and also directly after braking events.

The model is able to reproduce all three phases (free-flow, synchronised, and wide jams) observed in real traffic. Furthermore it shows a good agreement with detailed empirical single-vehicle data in all phases, e.g. for the auto- and cross-correlation functions defined in (1). The model passes also a rather sensitive test, namely it allows to reproduced the empirically observed coexistence of phases [52], especially the upstream propagation of wide jams through both free flow and synchronized traffic with constant velocity and without disturbing these states.

8 City traffic

At about the same time when Nagel and Schreckenberg introduced their CA model for highway traffic, another CA model for city traffic was suggested by Biham, Middleton and Levine (BML) [53]. This model is rather simplistic since it only consists of the intersections without any connecting streets. In order to allow a study of the interplay between signal periods and distance between intersections, a more realistic model was introduced later in [54].

8.1 BML model

In the BML model [53], each of the sites of a square lattice represents the intersection of a east-west street and a north-south street (see Fig. 12). All the streets parallel to the $\hat{X}$-direction of a Cartesian coordinate system are assumed to allow only single-lane east-bound traffic while all those parallel to the $\hat{Y}$-direction allow only single-lane north-bound traffic. In the initial state of the system, vehicles are randomly distributed among the streets. The states of east-bound vehicles are updated in parallel at every odd discrete time step whereas those of the north-bound vehicles are updated in parallel at every even timestep. The update rule is identical to that of the NaSch model with $v_{\max} = 1$ and $p = 0$: a vehicle moves forward one cell if and only if the cell in front is empty, otherwise the vehicle does not move at that timestep.

Computer simulations demonstrate that a first order phase transition takes place in the BML model at a finite non-vanishing density ρ_c, where the average velocity of the vehicles vanishes discontinuously signalling complete jamming. This jamming arises from the mutual blocking of the flows of east-bound and north-bound traffic at various different intersections [55,56].

Note that the dynamics of the BML model is fully deterministic and the randomness arises only from the random initial conditions [57]. As expected, for city traffic the interactions with the traffic lights are much more important than those with other vehicles.

At first sight the BML model may appear very unrealistic because the vehicles seem to hop from one intersection to the next. However, each unit of discrete time interval in the BML model might be interpreted as the time for which the traffic lights remain green (or red) before switching red (or green) simultaneously in a synchronized manner, and over that time scale each vehicle, which faces a green traffic light, gets an opportunity to move from j-th intersection to the $(j+1)$-th.

Various modifications of the original BML model have been studied, e.g. by allowing cars to change their direction of motion. We refer to [1] for a detailed list of these variants.

8.2 CS model

If one wants to develope a more detailed "fine-grained" description then one must first decorate each bond with $D-1$ $(D > 1)$ sites to represent $D-1$ cells in between each pair of successive intersections thereby modelling each segment of the streets in between successive intersections in the same manner in which the entire highway is modelled in the NaSch model. Then, one can follow the prescriptions of the NaSch model for describing the positions, speeds and accelerations of the vehicles as well as for taking into account the interactions among the vehicles moving along the same street. Moreover, one should flip the color of the traffic light periodically at regular intervals of T ($T \gg 1$) time steps where, during each unit of the discrete time interval every vehicle facing a green traffic light should get an opportunity to still move forward. Such a CA model of traffic in cities has been proposed recently [54]. The rules of updating have been formulated in such a way that, (a) a vehicle approaching an intersection can keep moving, even when the traffic light is red, until it reaches a cell immediately in front of which there is either a halting vehicle or an intersection; and (b) no grid-locking would occur in the absence of random braking.

Depending on the details of the rules, e.g. when cars are allowed to stop on the intersection, the model exhibits a gridlock transition similar to the BML model [54]. A typical gridlock configuration is shown in Fig. 12.

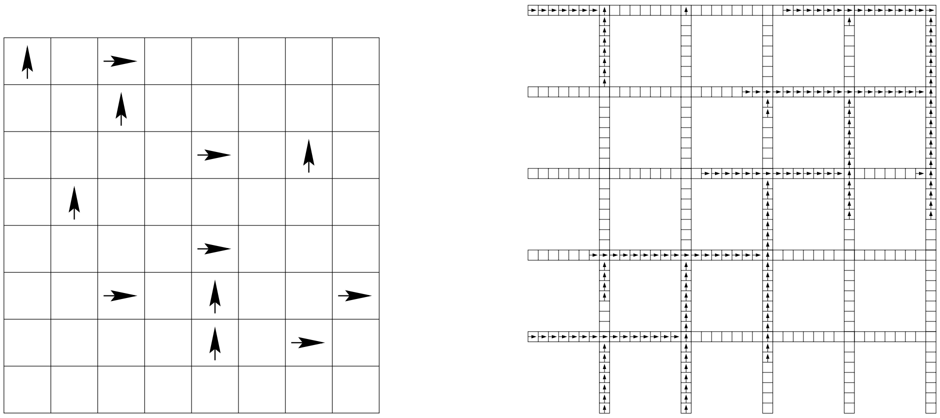

Fig. 12. Cellular automata models for city traffic: BML model (left) and CS model with $D = 8$ (right).

If the rules are modified slightly such that cars are not allowed to stop on the intersection when it is not clear that they can leave it in the next timestep, no gridlock occurs and one can study effects of different signal strategies. One can try to find the best strategy which leads to the largest flow for a given network topology [58]. In the following we will fix the signal length T which is supposed to be the same at all intersections. However, we allow the traffic lights to switch not at the same time, but with some offset to the neighbouring intersections.

In the simplest case, all traffic lights switch at the same time, like in the BML model. In this synchronized strategy the system behaves very similar to a single intersection and no additional gain can be obtained from the network topology.

In order to improve the performance of the network one can implement a green wave strategy. Here the traffic lights at successive intersections do not switch at the same time, but with a certain time delay $T_{\rm delay}$. The optimal $T_{\rm delay}$ corresponds to the time a vehicle needs from one intersection to the next one. Obviously green waves where almost no vehicle has to stop in front of a red traffic light can only be established at low densities. At large densities, jams will always exit. However, an improvement can still be obtained by choosing $T_{\rm delay}$ such that it corresponds to the time a jam needs to move (backwards!) from one intersection to the next. The jams are guided through the network such that the traffic lights are blocked when they are red anyway.

Finally, in [58] a random offset strategy has been tested. Here the delay time between successive intersections is not fixed, but chosen randomly. Surprisingly it is found that such strategies are very flexible and perform quite well for all densities. At high densities it leads to a larger flow than the synchronized strategy since some parts of the network are jammed whereas in others cars can move almost undisturbed.

8.3 Application: Online simulations

In this subsection we want to present briefly a possible application of the models discussed in this review to a real network of urban traffic.

The models can be used in order to obtain accurate information about the state of a traffic network. Typically, traffic data are collected only by locally fixed detectors (see Sec. 2) which are usually not installed on every road of the network, but spatially concentrated in the neighbourhood of intersections. In order to derive traffic information for those regions which are not covered by measurements, it is necessary to combine local traffic counts with the network structure. This is the basic idea of so-called online-simulations [59,60]. Local traffic counts serve as input for flow simulations in the considered network and provide network-wide information. An advantage of such a microscopic approach is that all aspects which have to be considered for the interpolation, like network structures and traffic lights, are directly incorporated into the simulation dynamics.

This strategy is implemented already for the city of Duisburg [60]. The results are available on the internet [61] in the form of a road-usage map (see Fig. 13). Related projects, sometimes even more ambitious, have been carried out for other urban [62,63] and highway models [64,65] (see also [4] for a more complete review).

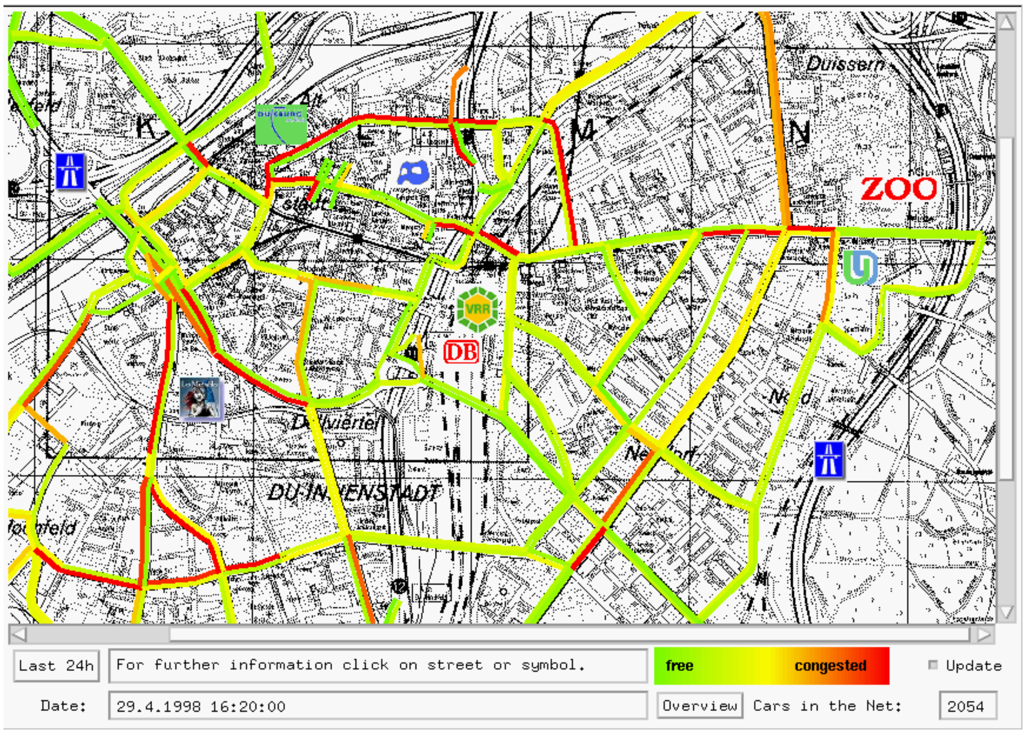

Fig. 13. Snapshot of an online simulation for the street network of the city of Duisburg. Different colours indicate different traffic densities.

9 Pedestrian dynamics

Pedestrian dynamics has not been studied as extensively as vehicular traffic, especially using a cellular automata approach. Due to its generically two-dimensional nature pedestrian motion is more difficult to describe in terms of simple models. On the other hand, these systems exhibit many interesting collective effects and self-organization phenomena (see [2] for an overview and a comprehensive list of references):

- **Jamming**: At large densities various kinds of jamming phenomena occur, e.g. when many people try to leave a large room at the same time. Other types of jamming occur in the case of counterflow.
- **Lane formation**: In counterflow, i.e. two groups of people moving in opposite directions, a kind of spontaneous symmetry breaking can occur. The motion of the pedestrians self-organizes in such a way that (dynamically varying) lanes are formed where people move in just one direction [66]. In this way, strong interactions with oncoming pedestrians are reduced and a higher walking speed is possible.
- **Oscillations**: In counterflow at bottlenecks, e.g. doors, one can observe oscillatory changes of the direction of motion. Once a pedestrian is able to pass the bottleneck it becomes easier for others to follow him in the same

direction until somebody is able to pass (e.g. through a fluctuation) the bottleneck in the opposite direction.
- **Patterns at intersections**: At intersections various collective patterns of motion can be formed. A typical example are short-lived roundabouts which make the motion more efficient. Even if these are connected with small detours the formation of these patterns can be favourable since they allow for a “smoother” motion.
- **Panics**: In panic situations many counter-intuitive phenomena (e.g. “faster-is-slower” and “freezing-by-heating” effects [67]) can occur. For a thorough discussion we refer to [68] and references therein.

In recent years, several models for the description of pedestrian dynamics have been suggested:

- **Social force models**: So far continuum models have been most successful in modelling pedestrian dynamics. An important example are the social force models (see e.g. [13,2,66] and references therein). Here pedestrians are treated as particles subject to long-ranged forces induced by the social behaviour of the individuals. This leads to (coupled) equations of motion similar to Newtonian mechanics. There are, however, important differences since, e.g., in general the third law (“actio = reactio”) is not fulfilled.
- **Active walker models**: So-called active walker models [69,70] have been used to describe the formation of human or animal trails etc. Here the walker leaves a trace by modifying the underground on his path. This modification is real in the sense that it could be measured in principle. For trail formation, vegetation is destroyed by the walker or animals (like ants) leave a chemical trace which can be detected by other animals.
- **Cellular automata**: Most CA models for pedestrian dynamics proposed so far are rather simple [71–73] and can be considered as generalizations of the BML model for city traffic (see Sec. 8.1). However, these models are not able to reproduce all the collective effects observed empirically. The same is true for more sophisticated discrete models, e.g. the model suggested by Gipps and Marksjös [75] or a disretized version of the social force model [76].

In [74] a new kind of CA model has been introduced which is - despite its simplicity - able to reproduce the observed collective effects. It takes its inspiration from the process of chemotaxis (see [77] for a review) as used e.g. by ants. They create a chemical trace to guide other individuals to food places. This is also the central idea of the active-walker models. In the approach of [74] the pedestrians also create a trace. In contrast to chemotaxis, however, this trace is only virtual. Its main purpose is to transform effects of long-ranged interactions (e.g. following people walking some distance ahead) into a local interaction (with the “trace”). This allows for a much more efficient simulation on a computer.

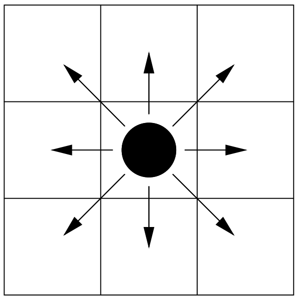

$M_{-1,-1}$	$M_{-1,0}$	$M_{-1,1}$
$M_{0,-1}$	$M_{0,0}$	$M_{0,1}$
$M_{1,-1}$	$M_{1,0}$	$M_{1,1}$

Fig. 14. A particle, its possible transitions and the associated matrix of preference $M = (M_{ij})$.

This basic idea is realized through the introduction of so-called floor fields. In its simplest version the model is defined on a array of quadratic cells. In one time step each pedestrian ('particle') can move to one of the nine neighbouring cells [9] in direction (i, j) (see Fig. 14). The transition probabilities now depend on the strength of the floor field in the target cell. A motion in the direction of large fields is preferred.

In fact it is advantaguous to introduce (at least) two different floor fields. The *static floor field* S is constant and takes into account the geometry of the system (building). In order to model people leaving a large room through a door one could use a static floor which increases with decreasing distance to the exit.

The second field, called *dynamic floor field* D, is just the virtual trace left by the pedestrians. It is modified by the presence of pedestrians and has its own dynamics, i.e. diffusion and decay. It is used to model a ("long-ranged") attractive interaction between the particles. Each pedestrian leaves a "trace", i.e. the floor field of occupied cells is increased. The dynamic floor field is also subject to diffusion and decay which leads to a dilution and finally the vanishing of the trace after some time.

Finally the transition probabilities depend on the preferred walking direction and speed of each individual. This is encoded in the *matrix of preferences* M. The entries of this matrix can be related to the preferred velocity vector and its longitudinal and transversal standard deviations (see [74] for details).

The *transition probability* p_{ij} in direction (i, j) is then determined by all three contributions. Schematically it is given by

$$p_{ij} = N M_{ij} D_{ij} S_{ij} (1 - n_{ij}). \tag{37}$$

N is a normalization factor to ensure $\sum_{(i,j)} p_{ij} = 1$ where the sum is over the nine possible target cells. The factor $1 - n_{ij}$, where n_{ij} is the occupation number

[9] i.e. she can also decide not to move

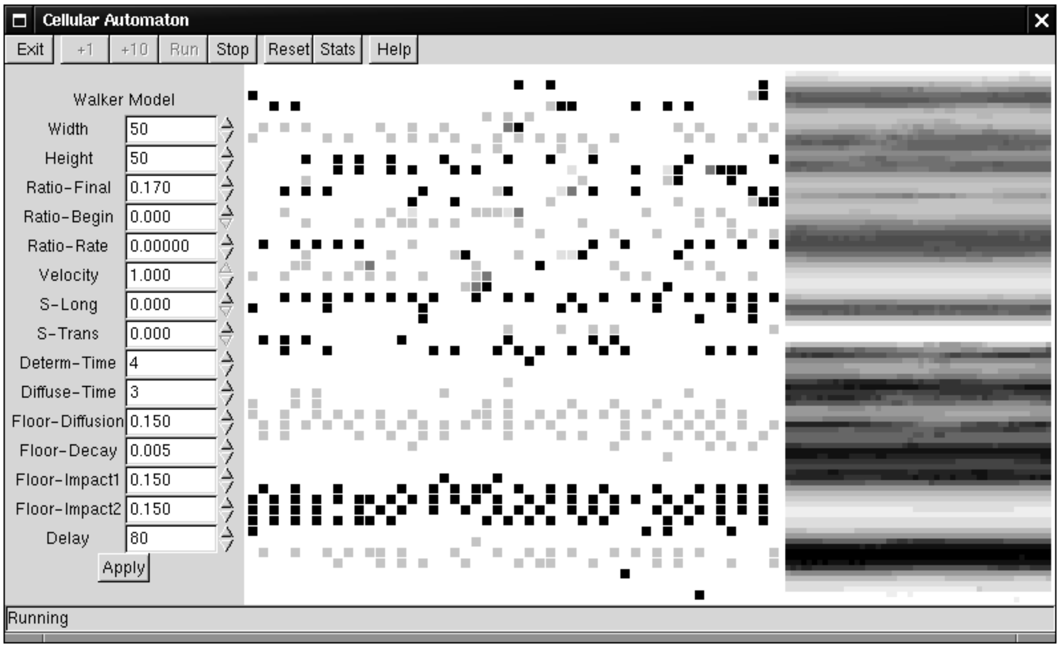

Fig. 15. Snapshot of a simulation using the new CA model for pedestrian dynamics. The left part shows the parameter control. The central window is the corridor and the light and dark squares are right- and left-moving pedestrians, respectively. The right part shows the floor fields for the two species.

of the neighbour cell in direction (i, j), takes into account that transitions to occupied cells are forbidden.

The details of the update rules can be found in [74]. There it is also shown that this model is very efficient in computer simulations. Pedestrian crowds of a few hundred people can be simulated 10 to 100 times faster than real time. More importantly the models allows to reproduce the empirically observed phenomena. As most most prominent example we want to discuss lane formation out of a randomly distributed group of pedestrians. As mentioned earlier this corresponds to a spontaneous breaking of the symmetry of the particle number distribution in space. Simulations show that an even as well as an odd number of lanes may be formed. The latter corresponds to a spontaneous breaking of the left-right symmetry of the system.

Fig. 15 shows simulations of a rectangular corridor which is populated by two species of pedestrians moving in opposite directions. Parallel to the direction of motion the existence of walls is assumed. Orthogonal to the direction of motion both periodic and open boundary conditions have been investigated. With periodic boundary conditions, the density of pedestrians is fixed for each run. It is ensured that the overall number of pedestrians is evenly divided by the numbers for the different species: with two species, one is moving to the left and the other to the right. For open boundaries, we fix the rate at which pedestrians enter the system at the boundaries. The pedestrians leave the system as soon as they reach the opposite end of the corridor.

Fig. 15 shows the graphical frontend running a simulation of a small periodic system. Lanes have already formed in the lower part of the corridor and can be spotted easily, both in the main window showing the cell contents and the small windows on the right showing the floor field intensity for the two species.

Apart from lane formation also oscillations of the direction of flow at doors and the formation of flow patterns at intersections have been found. Since the model captures the main phenomena correctly and is extremely efficient in computer simulations it might be an ideal tool for evacuation simulations [78].

10 Conclusions

We have tried to give an overview over the statistical physics aspects of traffic flow. The ability of simple cellular automaton models to reproduce many empirically observed properties has been emphasized. In its simplest version the NaSch model reproduces features like spontaneous jam formation and the basic structure of the fundamental diagram with a free flow and a congested phase. A simple generalization which includes a slow-to-start rule then allows to model the occurance of metastable states of high flow. In order to reproduce the full phase diagram, including synchronized traffic, more sophisticated models are necessary. Here not only the avoidance of crashes is important, but also the desire of the drivers for smooth and comfortable driving.

In this review many interesting aspects had to be left out. E.g. for practical applications one also has to be able to model multilane traffic and on- and off-ramps. Furthermore, there are surprising connections to many other phenomena and systems, e.g. granular flow, protein synthesis, computer networks, herding and flocking and even socio-economic systems. For a discussion of these relations we have to refer to the reviews [1,2].

I hope that this brief overview has convinced the reader that the investigation of traffic flow is a fascinating field, both for its pratical relevance and the insights into the physics of systems far from equilibrium.

Acknowledgements: I like to thank all my collaborators for all the valuable discussions over the last years. I also thank the organizers of the Altenberg summer school and its participants for their interest and all the questions, many of which I have tried to answer in this article.

References

[1] D. Chowdhury, L. Santen and A. Schadschneider: Phys. Rep. **329**, 199 (2000)

[2] D. Helbing: `cond-mat/0012229`

[3] B.S. Kerner: Phys. World **8**, 25 (1999)

[4] K. Nagel, J. Esser and M. Rickert: Annu. Rev. Comp. Phys. **7**, p. 151, ed. D. Stauffer (World Scientific, 2000)

[5] D.E. Wolf, M. Schreckenberg and A. Bachem (eds.): *Traffic and Granular Flow*, (World Scientific, Singapore, 1996)

[6] M. Schreckenberg and D.E. Wolf (eds.): *Traffic and Granular Flow '97*, (Springer, Singapore, 1998)

[7] D. Helbing, H.J. Herrmann, M. Schreckenberg and D. Wolf (eds.): *Traffic and Granular Flow 99*, (Springer, Berlin, 2000)

[8] B. S. Kerner and H. Rehborn: Phys. Rev. **E52**, R1297 (1996)

[9] L. Neubert, L. Santen, A. Schadschneider and M. Schreckenberg: Phys. Rev. **E60**, 6480 (1999)

[10] M.J. Lighthill and G.B. Whitham: Proc. Roy. Soc. Lond. **A229**, 281 (1955)

[11] B.S. Kerner and P. Konhäuser: Phys. Rev. **E48**, 2335 (1993)

[12] I. Prigogine and R. Herman: *Kinetic Theory of Vehicular Traffic*, (American Elsevier, New York, 1971)

[13] D. Helbing: *Verkehrsdynamik: Neue Physikalische Modellierungskonzepte*, (in German) (Springer, 1997)

[14] M. Bando, K. Hasebe, A. Nakayama, A. Shibata and Y. Sugiyama: Phys. Rev. **E51**, 1035 (1995)

[15] M. Treiber, A. Hennecke and D. Helbing: Phys. Rev. **E62**, 1805 (2000)

[16] K. Nagel and M. Schreckenberg: J. Physique I **2**, 2221 (1992)

[17] A Java applet for the simulation of the model can be found at `http://www.thp.uni-koeln.de/~as/as.html`.

[18] M.R. Evans and R.A. Blythe: these proceedings

[19] A. Schadschneider and M. Schreckenberg: J. Phys. **A26**, L679 (1993)

[20] M. Schreckenberg, A. Schadschneider, K. Nagel and N. Ito: Phys. Rev. **E51** 2339 (1995)

[21] A. Schadschneider and M. Schreckenberg: J. Phys. **A30**, L69 (1997)

[22] A. Schadschneider and M. Schreckenberg: J. Phys. **A31**, L225 (1998)

[23] A. Schadschneider: Eur. Phys. J. **B10**, 573 (1999)

[24] H.A. Gutowitz, J.D. Victor and B.W. Knight: Physica **28D**, 18 (1987)

[25] E.F. Moore: Proc. Symb. Appl. Math. **14**, 17 (1962)

[26] V. Privman (ed.): *Nonequilibrium Statistical Mechanics in One Dimension*, (Cambridge University Press, 1997)

[27] B. Schmittmann and R.P.K. Zia: *Statistical Mechanics of Driven Diffusive Systems*, in C. Domb and J.L. Lebowitz (eds.), *Phase Transitions and Crititcal Phenomena*, Vol. 17 (Academic Press, 1995)

[28] G.M. Schütz: *Exactly Solvable Models for Many-Body Systems*, in C. Domb and J.L. Lebowitz (eds.), *Phase Transitions and Crititcal Phenomena*, Vol. 19 (Academic Press, 2001)

[29] A.B. Kolomeisky, G. Schütz, E.B. Kolomeisky and J.P. Straley: J. Phys. **31**, 6911 (1998)

[30] V. Popkov, L. Santen, A. Schadschneider and G.M. Schütz: J. Phys. **A34**, L45 (2001)

[31] A. Schadschneider: Physica **A285**, 101 (2000)

[32] J. Krug: Braz. Jrl. Phys. **30**, 97 (2000) [cond-mat/9912411]

[33] M.R. Evans: Europhys. Lett. **36**, 13 (1996)

[34] M.R. Evans: J. Phys. **A30**, 5669 (1997).

[35] J. Krug and J.A. Ferrari: J. Phys. **A29**, 465 (1996)

[36] J. Krug: in [6], p. 285

[37] S.A. Janowsky and J.L. Lebowitz: Phys. Rev. A **45**, 618 (1992)

[38] S.A. Janowsky and J.L. Lebowitz: J. Stat. Phys. **77**, 35 (1994)

[39] S. Yukawa, M. Kikuchi and S. Tadaki: J. Phys. Soc. Japan, **63**, 3609 (1994)

[40] Z. Csahok and T. Vicsek: J. Phys. **A27**, L591 (1994)

[41] H. Emmerich and E. Rank: Physica **A216**, 435 (1995)

[42] W. Knospe, L. Santen, A. Schadschneider and M. Schreckenberg: in [6], p. 349

[43] T. Nagatani, J. Phys. Soc. Japan, **66**, 1928 (1997)

[44] A. Pottmeier, R. Barlovic, W. Knospe, A. Schadschneider and M. Schreckenberg: to appear in Physica **A**

[45] B. Eisenblätter, L. Santen, A. Schadschneider and M. Schreckenberg: Phys. Rev. **E57**, 1309 (1998)

[46] K. Nagel: Int. J. Mod. Phys. **C5**, 567 (1994)

[47] L. Roters, S. Lübeck and K.D. Usadel: Phys. Rev. **E61**, 3272 (2000) and references therein

[48] D. Chowdhury, J. Kertesz, K. Nagel, L. Santen and A. Schadschneider: Phys. Rev. **E61**, 3270 (2000)

[49] R. Barlovic, L. Santen, A. Schadschneider and M. Schreckenberg: Eur. Phys. J. **B5**, 793 (1998)

[50] W. Knospe, L. Santen, A. Schadschneider and M. Schreckenberg: `cond-mat/0107051` (to appear in Phys. Rev. **E**)

[51] W. Knospe, L. Santen, A. Schadschneider and M. Schreckenberg: J. Phys. **A33**, L477 (2000)

[52] B. S. Kerner: Networks and Spatial Economics **1**, 35 (2001)

[53] O. Biham, A.A. Middleton and D. Levine: Phys. Rev. **A46**, R6124 (1992)

[54] D. Chowdhury and A. Schadschneider: Phys. Rev. **E59**, R1311 (1999)

[55] S. Tadaki and M. Kikuchi: Phys. Rev. **E50**, 4564 (1994); J. Phys. Soc. Jap. **64**, 4504 (1995)

[56] H.S. Gupta and R. Ramaswamy: J.Phys. **A29**, L547 (1996)

[57] M. Fukui and Y. Ishibashi: J. Phys. Soc. Jap. **65**, 1871 (1996)

[58] E. Brockfeld, R. Barlovic, A. Schadschneider and M. Schreckenberg: `cond-mat/0107056` (to appear in Phys. Rev. **E**)

[59] J. Esser and M. Schreckenberg: Int. J. Mod. Phys. **C8**, 1025 (1997)

[60] J. Wahle, L. Neubert, J. Esser and M. Schreckenberg: Parallel Comp. **27**, 719 (2001)

[61] `http://www.traffic.uni-duisburg.de/OLSIM/`

[62] M. Rickert and K. Nagel: Int. J. Mod. Phys. **C8**, 483 (1997) (E: 1009)

[63] K. Nagel and C.L. Barrett: Int. J. Mod. Phys. **C8**, 505 (1997)

[64] M. Rickert and P. Wagner: Int. J. Mod. Phys. **C7**, 133 (1996)

[65] K. Nagel: Ph.D. thesis, Universität zu Köln (1995)

[66] D. Helbing and P. Molnar: Phys. Rev. **E51**, 4282 (1995)

[67] D. Helbing, I. Farkas and T. Vicsek: Phys. Rev. Lett. **84**, 1240 (2000)

[68] D. Helbing, I. Farkas and T. Vicsek: Nature **407**, 487 (2000)

[69] D. Helbing, F. Schweitzer, J. Keltsch and P. Molnar: Phys. Rev. **E56**, 2527 (1997)

[70] D. Helbing, J. Keltsch and P. Molnar: Nature **388**, 47 (1997)

[71] M. Fukui and Y. Ishibashi: J. Phys. Soc. Jpn. **68**, 2861 (1999)

[72] M. Muramatsu and T. Nagatani: Physica **A275**, 281 (2000)

[73] H. Klüpfel, T. Meyer-König, J. Wahle and M. Schreckenberg: in *Theory and Practical Issues on Cellular Automata*, S. Bandini, T. Worsch (Eds.), Springer (2000)

[74] C. Burstedde, K. Klauck, A. Schadschneider and J. Zittartz: Physica **A295**, 507 (2001)

[75] P.G. Gipps and B. Marksjös: Math. and Comp. in Simulation **27**, 95 (1985)

[76] K. Bolay: Diploma Thesis, Stuttgart University (1998)

[77] E. Ben-Jacob: Contemp. Phys. **38**, 205 (1997)

[78] A. Kirchner and A. Schadschneider: in preparation